Synthesis, Characterization, and Reactivity of Ferrous and Ferric Oxo/Peroxo Pivalate Complexes in Relation to Gif-Type Oxygenation of Substrates

Remle Çelenligil-Çetin,[†] Richard J. Staples,[‡] and Pericles Stavropoulos*,[†]

Department of Chemistry, Boston University, Boston, Massachusetts 02215, and Department of Chemistry and Chemical Biology, Harvard University, Cambridge, Massachusetts 02138

Received March 7, 2000

This study examines structural features and aspects of reactivity of Gif-type reagents, which depend on O_2/Zn to mediate oxidation of hydrocarbons. The reagents investigated derive from the use of iron complexes with the anion of the weak carboxylic acid Me_3CCO_2H (pivalic acid (PivH)) in pyridine/PivH. In these solutions, the known compound $[Fe_3O(O_2CCMe_3)_6(py)_3]$ is reduced by Zn to generate yellow-green $[Fe^{II}(O_2CCMe_3)_2(py)_4]$, which readily reverts to $[Fe_3O(O_2CCMe_3)_6(py)_3]$, and eventually to $[Fe_3O(O_2CCMe_3)_6(py)_3]^+$, upon exposure to dioxygen. All three species are equally well suited to mediate Gif-like oxygenation of substrates supported by O_2/Zn. $[Fe^{III}_3O(O_2CCMe_3)_6(L)_3]^+$ (L = H_2O, py) is converted by H_2O_2 to afford the hexairon(III) peroxo compounds $[Fe_6(O_2)(O)_2(O_2CCMe_3)_{12}(L)_2]$ (L = Me_3CCO_2H, py), which feature a $[Fe_6(\eta^2\text{-}\mu_4\text{-}O_2)(\mu_3\text{-}O)_2]$ core previously documented in the closely related $[Fe_6(O_2)(O)_2(O_2CPh)_{12}(H_2O)_2]$. A similar peroxo species, $[Fe_6(O_2)(O)_2(O_2CCMe_3)_2(O_2CCF_3)_{10}(H_2O)_2]$, is obtained upon replacing all pivalate ligands by trifluoroacetate groups with the exception of those pivalates that bridge between the two $[Fe_3O(O_2CCF_3)_5(H_2O)]^{2+}$ units. The structure of the $[Fe_6(O_2)(O)_2]$ core in these peroxo species is found to range from a recliner to a butterfly-type conformation. Reduction of $[Fe_6(O_2)(O)_2(O_2CCMe_3)_{12}(HO_2CCMe_3)_2]$ with $NaBH_4$ generates $[Na_2Fe_4(O)_2(O_2CCMe_3)_{10}(L)(L')]$ (L = CH_3CN, L′ = Me_2CO; L = L′ = Me_3CCO_2H), which feature a $[Na_2Fe_4(O)_2]$ core possessing a bent butterfly conformation of the $[Fe_4(O)_2]$ unit. Oxidation of the same peroxo complex by Ce^{IV} or $NOBF_4$ regenerates the oxo-bridged $[Fe_3O(O_2CCMe_3)_6(solv)_3]^+$ (solv = EtOH, H_2O, thf). Employment of the sterically encumbered 2-Me-5-Etpyridine provides the tetrairon compound $[Fe_4(O)_2(O_2CCMe_3)_8(2\text{-Me-5-Etpy})_2]$, which can be readily transformed upon treatment with H_2O_2 to the asymmetric peroxo complex $[Fe_6(O_2)(O)_2(O_2CCMe_3)_{12}(2\text{-Me-5-Etpy})_2]$. The peroxo-containing complexes oxidize both *cis*-stilbene and adamantane in either benzene or py/PivH, but only under forceful conditions and at very low yields. The low reactivity and high selectivity (tert/sec = 8) obtained in the oxidation of adamantane suggests that the present type of peroxo species is not directly involved in catalytic Gif-type oxygenations of adamantane.

Introduction

Hydrocarbon-oxidizing Gif-type systems[1] can be roughly divided into two categories: (i) those which require dioxygen and a reducing agent (usually Zn, but also metallic Fe or an electrochemical cathode) in the presence of an iron catalyst;[2] (ii) reagents which will only operate by employing Fe(II)/H_2O_2 or Fe(III)/H_2O_2 combinations.[3] This distinction is largely dictated by the electron-donor properties of a required carboxylic acid which is added into typical Gif solutions (pyridine/RCOOH 10:1 v/v) and/or coordinated to the iron reagent as the carboxylic acid anion. Ferrous sites featuring acetate[4] or, as shown in the present study, pivalate ligation (Piv, $Me_3CCO_2^-$), are dioxygen sensitive and would support O_2/Zn-dependent cycles, while the corresponding Fe(II) picolinate[5] and trifluoroacetate[6] species are stable to dioxygen (at least in pyridine) and would exclusively operate under H_2O_2. The former Fe(II) sites will also support H_2O_2-dependent oxygenations, albeit at very low, substoichiometric yields, apparently because, once oxidized, the corresponding ferric species would not activate H_2O_2. In the latter category of Gif reagents, a clear-cut mechanistic distinction between Fe(II)/H_2O_2 (radical) versus Fe(III)/H_2O_2 (nonradical) reagents has been proposed by Barton.[3] However, recent results[5c,6c] suggest that an argument in support of decoupling the cycles of these two reagents cannot be readily made, since several Fe(III) sites would easily regenerate Fe(II) species in the presence of excess H_2O_2.

From a mechanistic standpoint, two opposing pathways, a nonradical and a radical, have been proposed to explain the unusual selectivity of Gif reagents toward ketonization of

[†] Boston University.
[‡] Harvard University.

(1) (a) Barton, D. H. R.; Doller, D. *Acc. Chem. Res*. **1992**, *25*, 504−512. (b) Barton, D. H. R. *Aldrichim. Acta* **1990**, *23*, 3−11.
(2) Barton, D. H. R.; Bévière, S. D.; Chavasiri, W.; Csuhai, E.; Doller, D.; Liu, W.-G. *J. Am. Chem. Soc*. **1992**, *114*, 2147−2156.
(3) Barton, D. H. R.; Hu, B.; Taylor, D. K.; Rojas Wahl, R. U. *J. Chem. Soc., Perkin Trans. 2* **1996**, 1031−1041.
(4) (a) Singh, B.; Long, J. R.; Fabrizi de Biani, F.; Gatteschi, D.; Stavropoulos, P. *J. Am. Chem. Soc*. **1997**, *119*, 7030−7047. (b) Singh, B.; Long, J. R.; Papaefthymiou, G. C.; Stavropoulos, P. *J. Am. Chem. Soc*. **1996**, *118*, 5824−5825.
(5) (a) Balavoine, G.; Barton, D. H. R.; Boivin, J.; Gref, A. *Tetrahedron Lett*. **1990**, *3*, 659−662. (b) Tung, H.-C.; Kang, C.; Sawyer, D. T. *J. Am. Chem. Soc*. **1992**, *114*, 3445−3455. (c) Kiani, S.; Tapper, A.; Staples, R. J.; Stavropoulos, P. *J. Am. Chem. Soc*. **2000**, *122*, 7503−7517.
(6) (a) Balavoine, G.; Barton, D. H. R.; Boivin, J.; Gref, A.; Ozbalik, N.; Rivière, H. *J. Chem. Soc., Chem. Commun*. **1986**, 1727−1729. (b) Balavoine, G.; Barton, D. H. R.; Boivin, J.; Gref, A.; Ozbalik, N.; Rivière, H. *Tetrahedron Lett*. **1986**, *27*, 2849−2852. (c) Tapper, A. E.; Long, J. R.; Staples, R. J.; Stavropoulos, P. *Angew. Chem., Int. Ed.* **2000**, *39*, 2343−2346.

10.1021/ic000261+ CCC: $19.00
Published on Web 11/21/2000

hydrocarbons. Common to both mechanisms is the recognition that alkylhydroperoxide (ROOH) is the experimentally verifiable precursor[2] of the ketone (major product) and alcohol (minor amounts). Furthermore, both pathways account for the observation that the oxygen atoms in the alkylhydroperoxide are derived from dioxygen.[7] A distinctive feature of Barton's mechanism is that the assembly of alkylhydroperoxide is suggested to proceed via the usual alkyl (R−) and alkylperoxo (ROO−) precursors which, however, remain bound to the metal at all times. In addition, the active oxidant is presumed to be a high-valent Fe^{V}═O unit which abstracts hydrogen atoms from C−H bonds via concerted [2 + 2]-type addition.

Reservations on the applicability of this nonradical mechanism were first reported by Perkins,[7,8] and later substantiated by Minisci[9] and Ingold,[10] in a compelling body of work centered on Fe(III)/*t*-BuOOH systems. These reagents were initially considered to constitute a branch of the Gif family,[3] but as evidence favoring operation of a radical Haber−Weiss−Walling mechanism[11] accumulated, it was conceded[12] that *t*-BuOOH-dependent systems do not perform typical Gif chemistry. Minisci's work[13] stimulated a wider reconsideration of the Gif mechanism,[8] as other mainstream Gif reagents have also been suspected to operate via radical pathways. M. Newcomb and co-workers[14] have shown that at least one Gif reagent ($FeCl_3$/H_2O_2 in py/AcOH) oxidizes diagnostic radical-clock substrates via pathways involving diffusively free substrate radicals. Recent work in our laboratory, employing Gif reagents composed of iron picolinate[5c] or trifluoroacetate[6c] species and H_2O_2, has documented that both tertiary and secondary alkyl radicals are generated from substrates frequently used in Gif chemistry. Moreover, it has been shown that HO• radicals are responsible for the H-atom abstraction step under Ar, coupled to a more selective oxidant (most likely, substrate derived alkoxyl radicals) under partial pressures of dioxygen.

In the present study, we revisit those Gif-type reagents which are supported by O_2/Zn. A previous investigation[4] of hydrocarbon-oxidizing systems such as $[Fe_3O(O_2CCH_3)_6(py)_3]$ (or $[Fe(O_2CCH_3)_2(py)_4]$) coupled to sacrificial O_2/Zn in py/AcOH illustrated the complex nature of these solutions, and concluded that although structural analogies between isolable ferrous sites in Gif chemistry and corresponding sites in non-heme oxygenases (sMMO)[15] do exist, the functional aspects of Gif oxygenations are not consistent with the action of high-valent Fe═O units.[16] Based on a handful of product profiles, skepticism was also expressed[4] as to whether HO• radicals are the *sole* oxidizing species. However, no systematic effort was undertaken to search for carbon- and/or oxygen-centered radicals. Reported in the present study is a family of hydrocarbon-oxidizing Gif-type reagents composed of iron pivalate species, requiring O_2/Zn for turnover. Aspects of the relevant structural chemistry, along with stoichiometric oxygenations of substrates by isolable peroxo species, are discussed in this article. Mechanistic investigations of catalytic oxygenations, employing reagents described in this study, will be presented in due course.[17]

Experimental Section

General Considerations. All operations were performed under a pure dinitrogen atmosphere using Schlenk techniques on a gas/vacuum manifold or in an inert-atmosphere drybox (O_2, H_2O < 1 ppm). Hexane, petroleum ether, and toluene were distilled over Na, and THF and diethyl ether were distilled over Na/Ph_2CO. Acetonitrile and methylene chloride were distilled over CaH_2. Ethanol and methanol were distilled over the corresponding magnesium alkoxide, and acetone was distilled over drierite. All solvents were degassed by three freeze−pump−thaw cycles. Anhydrous pyridine (water < 0.005%), 2-methyl-5-ethylpyridine, and pivalic acid were purchased from Aldrich. Authentic *tert*-adamantylpyridines (2-(1-Ad)-py, 4-(1-Ad)-py)[18] and *sec*-adamantylpyridines (2-(2-Ad)-py, 4-(2-Ad)-py)[18] were prepared by photolysis of suitable adamantyl-radical-generating precursors in the presence of protonated pyridine according to literature procedures.

Preparation of Compounds. $[Fe_3O(O_2CCMe_3)_6(OH_2)_3]Cl\cdot 2H_2O\cdot CHCl_3$ (1). To an aqueous solution of $NaHCO_3$ (4.10 g, 48.0 mmol) was added pivalic acid (4.90 g, 48.0 mmol) while stirring. This solution was gently heated until the effervescence (CO_2) ceased. Upon dropwise addition of this solution to an aqueous solution of $FeCl_3\cdot 6H_2O$ (6.49 g, 24.0 mmol), an orange-red suspension was generated. The mixture was stirred for about 4 h filtered through a suction funnel, and the precipitate was allowed to dry overnight under vacuum. The so obtained orange solid was dissolved in diethyl ether, and the solution was filtered to remove any undissolved material. The ethereal dark red solution was allowed to slowly evaporate upon standing in air to afford red hexagonal crystals overnight (5.12 g, 73%). Crystals suitable for X-ray analysis can be obtained from chloroform. ^{1}H NMR (CD_2Cl_2): δ 10.99 (s, br, 18H, $(CH_3)_3CCO_2$), 8.04 (s, br, 36H, $(CH_3)_3CCO_2$), 4.64 (s, br, 9H, $(CH_3)_3CCO_2$), 1.74 (s, br, 6H, H_2O). Anal. Calcd for $C_{30}H_{60}Fe_3O_{16}Cl$: C, 40.96; H, 6.87. Found: C, 40.92; H, 6.86.

$[Fe_3O(O_2CCMe_3)_6(py)_3]Cl$ (2). Compound **1** (0.43 g, 0.48 mmol) was dissolved in the minimum amount of pyridine (5.0 mL), and the mixture was heated during slow evaporation under vacuum. The resulting greenish-black solid was redissolved in pyridine, the solution was filtered, and diethyl ether was allowed to diffuse into the filtrate at −10 °C to afford green-black crystals of **2** (0.14 g, 27%). ^{1}H NMR ($CDCl_3$): δ 39.64 (s, 6H, 2-*H*-py), 27.98 (s, 3H, 4-*H*-py), 18.23 (s, 6H, 3-*H*-py), 10.62 (s, 24H, $(CH_3)_3CCO_2$), 8.19 (s, 18H, $(CH_3)_3CCO_2$), 4.91 (s, 12H, $(CH_3)_3CCO_2$). Anal. Calcd for $C_{45}H_{69}N_3Fe_3O_{13}Cl$: C, 50.84; H, 6.54; N, 3.95. Found: C, 50.67; H, 6.68; N, 3.84.

$[Fe(O_2CCMe_3)_2(py)_4]$ (3). Iron powder (0.980 mg, 17.5 mmol) was vigorously stirred in a solution of pyridine (15 mL) and pivalic acid (3.57 g, 35.0 mmol) upon refluxing for 5 days. The so obtained yellow-brown solution was filtered and the filtrate afforded green crystals upon cooling at −20 °C. ^{1}H NMR (CD_2Cl_2): δ 48.99 (s, br, 8H, 2-*H*-py), 18.99 (s, 8H, 3-*H*-py), 11.12 (s, 4H, 4-*H*-py), 8.76 (s, 18H, $(CH_3)_3CCO_2$). Anal. Calcd for $C_{30}H_{38}N_4FeO_4$: C, 62.72; H, 6.67; N, 9.75. Found: C, 62.54; H, 6.74; N, 9.88.

(7) Knight, C.; Perkins, M. J. *J. Chem. Soc., Chem. Commun*. **1991**, 925−927.
(8) Perkins, M. J. *Chem. Soc. Rev*. **1996**, 229−236.
(9) (a) Minisci, F.; Fontana, F.; Araneo, S.; Recupero, F.; Banfi, S.; Quici, S. *J. Am. Chem. Soc*. **1995**, *117*, 226−232. (b) Minisci, F.; Fontana, F.; Araneo, S.; Recupero, F. *J. Chem. Soc., Chem. Commun*. **1994**, 1823−1824. (c) Minisci, F.; Fontana, F. *Tetrahedron Lett*. **1994**, *35*, 1427−1430.
(10) (a) Snelgrove, D. W.; MacFaul, P. A.; Ingold, K. U.; Wayner, D. D. M. *Tetrahedron Lett*. **1996**, *37*, 823−826. (b) Ingold, K. U.; MacFaul, P. A. In *Biomimetic Oxidations Catalyzed by Transition Metal Complexes*; Meunier, B., Ed.; Imperial College Press: London, 1999; pp 45−89.
(11) (a) Walling, C. *Acc. Chem. Res*. **1998**, *31*, 155−157. (b) Walling, C. *Acc. Chem. Res*. **1975**, *8*, 125−131.
(12) (a) Barton, D. H. R. *Synlett* **1997**, 229−230. (b) Barton, D. H. R.; Le Gloahec, V. N.; Patin, H.; Launay, F. *New J. Chem*. **1998**, *22*, 559−563. (c) Barton, D. H. R.; Le Gloahec, V. N.; Patin, H. *New J. Chem*. **1998**, *22*, 565−568.
(13) Minisci, F.; Fontana, F.; Araneo, S.; Recupero, F.; Zhao, L. *Synlett* **1996**, 119−125.
(14) Newcomb, M.; Simakov, P. A.; Park, S.-U. *Tetrahedron Lett*. **1996**, *37*, 819−822.
(15) (a) Choi, S.-Y., Eaton, P. E.; Hollenberg, P. F.; Liu, K. E.; Lippard, S. J.; Newcomb, M.; Putt, D. A.; Upadhyaya, S. P.; Xiong, Y. *J. Am. Chem. Soc*. **1996**, *118*, 6547−6555. (b) Liu, K. E.; Johnson, C. C.; Newcomb, M.; Lippard, S. J. *J. Am. Chem. Soc*. **1993**, *115*, 939−947.
(16) (a) Newcomb, M.; Le Tadic-Biadatti, M.-H.; Chestney, D. L.; Roberts, E. S.; Hollenberg, P. F. *J. Am. Chem. Soc*. **1995**, *117*, 12085−12091. (b) Atkinson, J. K.; Hollenberg, P. F.; Ingold, K. U.; Johnson, C. C.; Le Tadic, M.-H.; Newcomb, M.; Putt, D. A. *Biochemistry* **1994**, *33*, 10630−10637.
(17) Çelenligil-Çetin, R.; Stavropoulos, P. Manuscript in preparation.
(18) Barton, D. H. R.; Halley, F.; Ozbalik, N.; Schmitt, M.; Young, E.; Balavoine, G. *J. Am. Chem. Soc*. **1989**, *111*, 7144−7149.

Table 1. Crystallographic Data[a] for $[Fe(Piv)_2(py)_4]$ (**3**), $[Fe_6(O_2)(O)_2(Piv)_{12}(PivH)_2]$ (**4**), $[Fe_6(O_2)(O)_2(Piv)_{12}(py)_2]\cdot 0.5Me_2CO$ (**5**), $[Fe_6(O_2)(O)_2(TFA)_{10}(Piv)_2(H_2O)_2]\cdot 2Me_2CO\cdot EtOH$ (**6**), $[Na_2Fe_4(O)_2(Piv)_{10}(CH_3CN)(Me_2CO)]$ (**7**), and $[Na_2Fe_4(O)_2(Piv)_{10}(PivH)_2]\cdot 4CH_2Cl_2$ (**8**)

	3	**4**	**5**	**6**	**7**	**8**
formula	$C_{30}H_{38}FeN_4O_4$	$C_{70}H_{128}Fe_6O_{32}$	$C_{71.5}H_{121}Fe_6N_2O_{28.5}$	$C_{38}H_{40}F_{30}Fe_6O_{33}$	$C_{55}H_{99}Fe_4NNa_2O_{23}$	$C_{64}H_{116}Cl_8Fe_4Na_2O_{26}$
formula wt	574.50	1816.82	1799.80	1929.80	1411.73	1854.55
crystal system	monoclinic	triclinic	monoclinic	triclinic	monoclinic	monoclinic
space group	*C*2/*c*	$P\bar{1}$	$P2_1/c$	$P\bar{1}$	*Cc*	*C*2/*c*
Z	4	2	4	2	4	4
a, Å	9.0876(3)	13.039(3)	21.9379(5)	13.1278(5)	19.430(1)	22.510(6)
b, Å	17.2861(6)	13.667(3)	18.7231(7)	13.1794(5)	19.062(3)	14.196(5)
c, Å	19.0500(7)	15.403(3)	23.721(1)	25.0769(6)	19.859(4)	30.117(7)
α, deg	90	112.605(8)	90	75.731(2)	90	90
β, deg	99.866(1)	111.824(9)	99.235(4)	87.745(2)	91.06(1)	104.15(1)
γ, deg	90	90.78(1)	90	61.218(1)	90	90
V, Å^3	2948.3(2)	2312.9(8)	9617.1(6)	3669.3(2)	7354(2)	9332(5)
T, K	213(2)	213(2)	213(2)	213(2)	213(2)	213(2)
color	green	red-black	red-black	red-black	red-brown	red-brown
d_{calc}, g/cm^3	1.294	1.303	1.243	1.747	1.275	1.320
μ, mm^{-1}	0.552	0.989	0.948	1.309	0.851	0.912
$R1$[b] (wR_2[c]), %	5.62 (12.28)	7.20 (20.09)	8.44 (20.57)	10.15 (24.35)	4.30 (11.88)	8.44 (16.86)

[a] Obtained with graphite monochromated Mo Kα ($\lambda = 0.710\ 73$ Å) radiation. [b] $R1 = \sum||F_o| - |F_c||/\sum|F_o|$. [c] $wR_2 = \{\sum[w(F_o^2 - F_c^2)^2/\{\sum[w(F_o^2)^2]\}^{1/2}$.

$[Fe_6(O_2)(O)_2(O_2CCMe_3)_{12}(HO_2CCMe_3)_2]$ (4). To a dark-red ethereal solution of **1** (0.88 g, 0.99 mmol) was added H_2O_2 (0.5 mL, aqueous 30%). After stirring for about 1 h the reddish-black solution was poured over water. The extracted ether layer, which was dried over anhydrous $MgSO_4$, was allowed to slowly evaporate upon standing partially open to air. Reddish-black crystals of **4** (0.67 g, 79%) were collected the following day. ^{1}H NMR (CD_2Cl_2): δ 8.19 (s, br, 18H, (CH_3)$_3$CCO$_2$), 6.94 (s, br, 72H, (CH_3)$_3$CCO$_2$), 6.25 (s, br, 18H, (CH_3)$_3$CCO$_2$), 1.29 (s, br, 18H, (CH_3)$_3$CCO$_2$). Anal. Calcd for $C_{70}H_{128}Fe_6O_{32}$: C, 46.28; H, 7.10. Found: C, 46.54; H, 7.15.

$[Fe_6(O_2)(O)_2(O_2CCMe_3)_{12}(py)_2]\cdot 0.5Me_2CO$ (5). To a black acetone (10.0 mL)/ether (1.0 mL) solution of **2** (0.88 g, 0.83 mmol) was added H_2O_2 (0.5 mL, aqueous 30%). After stirring for about 1 h the reddish-black solution was poured over water. The extracted organic layer, which was dried over anhydrous $MgSO_4$, was allowed to evaporate upon standing partially open to air. Reddish-black crystals were collected the following day (0.08 g, 16%). ^{1}H NMR (CD_2Cl_2): δ 9.08 (s, br, 2-*H*-py), 8.24 (s, br, 18H, (CH_3)$_3$CCO$_2$), 7.42 (s, br, 3-*H*-py), 6.99 (s, br, 72H, (CH_3)$_3$CCO$_2$), 6.28 (s, br, 4-*H*-py), 6.09 (s, br, 18H, (CH_3)$_3$CCO$_2$), 2.85 (s, br, (CH_3)$_2$CO). Anal. Calcd for $C_{71.5}H_{121}N_2Fe_6O_{28.5}$: C, 47.72; H, 6.78; N, 1.56. Found: C, 47.88; H, 6.69; N, 1.54.

$[Fe_6(O_2)(O)_2(O_2CCMe_3)_2(O_2CCF_3)_{10}(H_2O)_2]\cdot 2Me_2CO\cdot EtOH$ (6). To a red-black solution of **4** (0.133 g, 0.073 mmol) in CH_2Cl_2 (50.0 mL, EtOH stabilized) was added dropwise CF_3COOH (0.08 mL, 1.02 mmol). The mixture was stirred for 2 days, and the filtrate was then layered with equal amount of hexane/acetone. Upon standing at −10 °C, the solution afforded within 1 week red-black crystals of **6** (49 mg, 34%). ^{1}H NMR ($CDCl_3$): δ 8.89 (s, br, 18H, (CH_3)$_3$CCO$_2$), 3.60 (br, 2H, CH_3CH_2OH), 2.15 (s, 12H, (CH_3)$_2$CO), 1.8 (s, 4H, H_2O), 1.6 (br, 3H, CH_3CH_2OH). Anal. Calcd for $C_{38}H_{40}O_{33}Fe_6F_{30}$: C, 23.65; H, 2.09; F, 29.53. Found: C, 23.70; H, 1.82; F, 28.84.

$[Na_2Fe_4(O)_2(O_2CCMe_3)_{10}(CH_3CN)(Me_2CO)]$ (7). A dark-red ethereal solution of **1** (0.66 g, 0.75 mmol) was stirred with $NaOCH_3$ (0.06 g, 1.08 mmol). To this mixture was added H_2O_2 (10 drops ≈ 0.5 mL, aqueous 30%). After about 1 h of stirring, the solution was filtered and evaporated to dryness under vacuum. The red solid so obtained was dissolved in a mixture of acetone (5.0 mL) and acetonitrile (5.0 mL), the solution was filtered, and the filtrate was allowed to evaporate slowly to afford red-brown crystals of **7** (0.66 g, 15%). ^{1}H NMR ($CDCl_3$): δ 8.16 (s, br, 18H, (CH_3)$_3$CCO$_2$), 7.75 (s, br, 18H, (CH_3)$_3$CCO$_2$), 5.95 (s, br, 36H, (CH_3)$_3$CCO$_2$), 2.15 (s, br, 6H, (CH_3)$_2$CO), 1.99 (s, br, 3H, CH_3CN), 1.55 (s, br, 18H, (CH_3)$_3$CCO$_2$). Anal. Calcd for $C_{55}H_{99}N_1Fe_4Na_2O_{23}$: C, 46.79; H, 7.07; N, 0.99; Na, 3.26. Found: C, 46.43; H, 7.12; N, 0.97; Na, 3.32.

$[Na_2Fe_4(O)_2(O_2CCMe_3)_{10}(HO_2CCMe_3)_2]\cdot 4CH_2Cl_2$ (8). Compound **4** (0.195 g, 0.107 mmol) and $NaBH_4$ (0.063 g, 1.66 mmol) were vigorously stirred in degassed CH_2Cl_2 (50 mL) for 4 days. The resulting orange-brown solution was filtered to remove any unreacted $NaBH_4$. The volume of the filtrate was reduced (10 mL) under vacuum, and the solution was stored at −20 °C to afford red-brown crystals of **8** (33 mg, 11%) in 2 weeks. ^{1}H NMR ($CDCl_3$): δ 8.89 (s, 18H, (CH_3)$_3$CCO$_2$), 7.79 (s, 18H, (CH_3)$_3$CCO$_2$), 5.83 (m, br, 36H, (CH_3)$_3$CCO$_2$), 5.28 (s, 2H, CH_2Cl_2), 2.98 (s, 18H, (CH_3)$_3$CCO$_2$), 1.23 (m, br, 18H, (CH_3)$_3$CCO$_2$). Anal. Calcd for $C_{64}H_{118}Cl_8Fe_4Na_2O_{26}$: C, 41.40; H, 6.41; Cl, 15.28; Na, 2.48. Found: C, 41.62; H, 6.53; Cl, 15.42; Na, 2.39.

$[Fe_4(O)_2(O_2CCMe_3)_8(2\text{-Me-5-Etpy})_2]\cdot 2CH_3CN$ (9). To compound **1** (3.5 g, 3.96 mmol) was added 2-Me-5-Etpy (1.0 mL, 7.6 mmol (stench)). The resulting black mixture was diluted and stirred overnight in a solution of CH_3CN (1 mL) and diethyl ether (10 mL). This was filtered and dried over anhydrous $MgSO_4$. The brownish-red filtrate was allowed to slowly evaporate upon standing partially open to air to afford red-black crystals of **9** (3.1 g, 79%). ^{1}H NMR ($CDCl_3$): δ 20.63 (br), 20.17 (br), 11.03 (s, br, 18H, (CH_3)$_3$CCO$_2$), 8.40 (s, br, 18H, (CH_3)$_3$CCO$_2$), 8.15 (s, br, 18H, (CH_3)$_3$CCO$_2$), 7.64 (s, br, 18H, (CH_3)$_3$CCO$_2$), 4.63 (br), 2.74 (br), 1.68 (br). Anal. Calcd for $C_{60}H_{100}N_4Fe_4O_{18}$: C, 51.89; H, 7.26; N, 4.03. Found: C, 51.71; H, 7.14; N, 3.98.

$[Fe_6(O_2)(O)_2(O_2CCMe_3)_{12}(2\text{-Me-5-Etpy})_2]$ (10). To a black solution of **9** (0.88 g, 0.67 mmol) in acetone (10.0 mL)/ether (1.0 mL) was added H_2O_2 (0.5 mL, aqueous 30%). After stirring for about 1 h the reddish-black solution was poured over water. The extracted ethereal layer, which was dried over anhydrous $MgSO_4$, was allowed to slowly evaporate upon standing partially open to air. Reddish-black crystals of **10** were collected the following day (0.07 g, 7%). ^{1}H NMR (CD_2Cl_2): δ 9.6 (br), 8.19 (s, br, 18H, (CH_3)$_3$CCO$_2$), 7.42 (br), 6.95 (s, br, 63−72H, (CH_3)$_3$CCO$_2$), 6.24 (s, br, 18H, (CH_3)$_3$CCO$_2$), 2.62 (br), 2.47 (br), 1.25 (s, 18H, (CH_3)$_3$CCO$_2$). Anal. Calcd for $C_{76}H_{130}N_2Fe_6O_{28}$: C, 49.21; H, 7.06; N, 1.51. Found: C, 49.34; H, 7.11; N, 1.54.

General Procedure for the Reaction of the Peroxo Species with (i) *cis*-Stilbene. Compound **4** or **5** (0.0028 mmol), *cis*-stilbene (0.0006 g, 0.0033 mmol), and the internal standard hexamethylbenzene (0.0006 g, 0.0037 mmol) were dissolved in C_6D_6 (0.5 mL) in an NMR tube. The tube was then flame sealed and kept at 70 °C. The formation of oxidation products was monitored by ^{1}H NMR by following the signal for the olefinic protons in *cis*-stilbene (δ 6.61), *cis*-stilbene oxide (δ 4.21), and *trans*-stilbene oxide (δ 3.78), as well as that for the aldehyde proton of benzaldehyde (δ 9.79). The ratio of **4** (or **5**) over *cis*-stilbene was varied from 1:1 to 1:2 while keeping the concentration of the iron compound constant.

(ii) Adamantane. Compound **4** (0.1 mmol) was dissolved in py (10.0 g)/PivH (1.0 g), thus being transformed to **5**. To this solution, adamantane was added (0.1 mmol) and the solution was kept at 66 °C in a closed flask under inert atmosphere. An aliquot was periodically withdrawn from this solution and analyzed by GC.

X-ray Structure Determinations. Crystallographic data for compounds **3**−**10** for which structures were determined are listed in Tables

Table 2. Crystallographic Data[a] for $[Fe_4(O)_2(Piv)_8(2\text{-Me-5-Etpy})_2]\cdot 2CH_3CN$ (**9**), and $[Fe_6(O_2)(O)_2(Piv)_{12}(2\text{-Me-5-Etpy})_2]$ (**10**)

	9	**10**
formula	$C_{60}H_{100}Fe_4N_4O_{18}$	$C_{76}H_{130}Fe_6N_2O_{28}$
formula wt	1388.84	1854.92
crystal system	monoclinic	monoclinic
space group	$P2_1/c$	$P2_1/n$
Z	4	4
a, Å	18.035(4)	16.3537(2)
b, Å	18.404(3)	23.0716(2)
c, Å	22.445(3)	26.5332(3)
α, deg	90	90
β, deg	94.093(9)	101.270(1)
γ, deg	90	90
V, Å^3	7431(2)	9818.1(2)
T, K	213(2)	213(2)
color	red-black	red-black
d_{calc}, g/cm^3	1.240	1.255
μ, mm^{-1}	0.828	0.931
$R1$[b] (wR_2[c]), %	8.55 (22.16)	4.61 (11.80)

[a] Obtained with graphite monochromated Mo Kα ($\lambda = 0.710\ 73$ Å) radiation. [b] $R1 = \sum||F_o| - |F_c||/\sum|F_o|$. [c] $wR_2 = \{\sum[w(F_o^2 - F_c^2)^2]/\sum[w(F_o^2)^2]\}^{1/2}$.

1 and 2. Crystallographic data for compounds **1** and $[Fe_3O(O_2CCMe_3)_6(EtOH)_2(H_2O)](NO_3)\cdot EtOH$ are reported as Supporting Information. Single crystals were picked from the crystallization vessel (coated with Paratone-N oil if necessary due to air sensitivity or desolvation), mounted on a glass fiber using grease, and transferred to a Siemens (Bruker) SMART CCD (charge coupled device) based diffractometer equipped with an LT-2 low-temperature apparatus operating at 213 K. Data were measured using omega scans of 0.3° per frame for 30 s such that a hemisphere was collected. A total of 1271 frames were collected with a maximum resolution of 0.75 Å (0.80 Å for **9**, 0.90 Å for **10**). The first 50 frames were recollected at the end of data collection to monitor for decay. Cell parameters were retrieved using SMART software[19] and refined using the SAINT software[20] which corrects for Lp and decay. Absorption corrections were applied using SADABS[21] supplied by George Sheldrick. The structures were solved by the direct method using the SHELXS-97[22] program and refined by least-squares method on F^2, SHELXL-97,[23] incorporated in SHELXTL-PC V 5.10.[24]

The structures were solved in the space groups specified in Tables 1 and 2 by analysis of systematic absences. All non-hydrogen atoms were refined anisotropically. For **3** (Supporting Information), hydrogens were located by difference Fourier maps and refined isotropically. For **4**−**10**, hydrogens were calculated by geometrical methods and refined as a riding model. The crystals used for the diffraction studies showed no decomposition during data collection. Several wR_2 values were high, as all compounds experienced large thermal motion due to the presence of $-C(CH_3)_3$ and $-CF_3$ groups. In compounds **1** and **5**, solvent molecules were also disordered. All drawings (Figures 1−8) are provided at 50% probability ellipsoids.

Other Physical Measurements. ^{1}H and ^{13}C NMR spectra were recorded on Varian XL-400 and JEOL GSX-270 NMR spectrometers, respectively. The isotropically shifted peaks for the iron-containing compounds were assigned when possible based on chemical shift, integration, and selective deuteration. FT-IR spectra were obtained on a Perkin-Elmer 1800 spectrometer. UV−vis spectra were obtained on a Hewlett-Packard 8452A diode array spectrometer. EI and CI mass spectra were obtained on a Finnigan MAT-90 mass spectrometer. Microanalyses were done by H. Kolbe, Mikroanalytisches Laboratorium, Mülheim an der Ruhr, Germany, and by Quantitative Technologies Inc., Whitehouse, NJ.

Results and Discussion

Synthesis and Characterization of Compounds. (i) Fe^{II}- and $[Fe^{III}_2Fe^{II/III}O]$-Containing Species. Entry into the chemistry of iron pivalate compounds can be achieved starting from triangular oxo-centered $[Fe_3O(O_2CCMe_3)_6(L)_3]^{+/0}$ species. The all-ferric compound has been previously documented[25,26] in $[Fe_3O(O_2CCMe_3)_6(L)_3](ClO_4)$ (L = H_2O, py) and $[Fe_3O(O_2CCMe_3)_6(MeOH)_3]Cl$, while the mixed-valent $[Fe_3O]^{6+}$ core has been isolated[26] in $[Fe_3O(O_2CCMe_3)_6(L)_3]$ (L = Me_3CCO_2H, py). The methanol adduct has been reported[27] to mediate dioxygen-dependent epoxidation of olefinic alcohol acetates. The pyridine and MeOH adducts noted above have been crystallographically characterized.[26]

Ferric pivalate species, which are found[17] to mediate Gif-type oxygenation of hydrocarbons in py/PivH (10:1 w/w), are best represented by $[Fe_3O(O_2CCMe_3)_6(py)_3]Cl$ (**2**), prepared in the present study via replacement of water in the corresponding water adduct by pyridine. The water adduct is crystallized from chloroform as $[Fe_3O(O_2CCMe_3)_6(H_2O)_3]Cl\cdot 2H_2O\cdot CHCl_3$ (**1**) and features a structure (Supporting Information) with crystallographically imposed D_3 symmetry. The central oxygen atom of the Fe_3O core resides in the plane of the metal atoms on a perpendicular C_3 axis. In contrast, the corresponding oxygen atom in the structure of $[Fe_3O(O_2CCMe_3)_6(MeOH)_3]Cl$ lies 0.24 Å off one side of the plane which is defined by the three ferric sites.[28]

Reduction of $[Fe_3O(O_2CCMe_3)_6(py)_3]Cl$ (**2**) or $[Fe_3O(O_2CCMe_3)_6(py)_3]$ by excess Zn dust in pyridine generates yellow-green solutions from which the air-sensitive $[Fe^{II}(O_2CCMe_3)_2(py)_4]$ (**3**) is isolated in good yields. Compound **3**, which can also be prepared pure by stirring Fe powder with 2 equiv of PivH in pyridine under reflux, reveals a structure (Supporting Information) which has now been documented in our laboratory for a number of other *trans*-$[Fe^{II}(O_2CCR_3)_2(py)_4]$ (R = H, F) complexes.[4,6c] The solid-state structure is retained in solution (py, CH_2Cl_2) as indicated by ^{1}H NMR data, although in non-pyridine solvents the compound becomes exceedingly air sensitive, suggesting that small amounts of the known[29] five-coordinate species $[Fe^{II}_2(O_2CCMe_3)_4(py)_2]$ may be present in equilibrium.

Exposure of **3** to dioxygen in pyridine readily regenerates $[Fe_3O(O_2CCMe_3)_6(py)_3]$, which, in turn, is slowly oxidized to $[Fe_3O(O_2CCMe_3)_6(py)_3]^+$. As shown elsewhere,[17] all three species can independently support oxygenation of adamantane by O_2/Zn (or H_2O_2, albeit at substoichiometric yields), presumably due to their rapid interconversion and generation of the

(19) *SMART V 5.050 (NT) Software for the CCD Detector System*; Bruker Analytical X-ray Systems: Madison, WI, 1998.
(20) *SAINT V 5.01 (NT) Software for the CCD Detector System*; Bruker Analytical X-ray Systems: Madison, WI, 1998.
(21) *SADABS Program for Absorption Corrections Using Siemens CCD Based on the Method of Robert Blessing*; Blessing, R. H. *Acta Crystallogr., Sect. A* **1995**, *A51*, 33−38.
(22) Sheldrick, G. M. *SHELXS-97 Program for the Solution of Crystal Structure*; University of Göttingen: Göttingen, Germany, 1997.
(23) Sheldrick, G. M. *SHELXL-97 Program for the Refinement of Crystal Structure*; University of Göttingen: Göttingen, Germany, 1997.
(24) *SHELXTL 5.10 (PC−Version) Program Library for Structure Solution and Molecular Graphics*; Bruker Analytical X-ray Systems: Madison, WI, 1998.
(25) Bond, A. M.; Clark, R. J. H.; Humphrey, D. G.; Panayiotopoulos, P.; Skelton, B. W.; White, A. H. *J. Chem. Soc., Dalton Trans.* **1998**, 1845−1852.
(26) Wu, R.; Poyraz, M.; Sowrey, F. E.; Anson, C. E.; Wocadlo, S.; Powell, A. K.; Jayasooriya, U. A.; Cannon, R. D.; Nakamoto, T.; Katada, M.; Sano, H. *Inorg. Chem.* **1998**, *37*, 1913−1921.
(27) Ito, S.; Inoue, K.; Matsumoto, M. *J. Am. Chem. Soc.* **1982**, *104*, 6450−6452.
(28) Blake, A. B.; Fraser, L. R. *J. Chem. Soc., Dalton Trans.* **1975**, 193−197.
(29) Randall, C. R.; Shu, L.; Chiou, Y. M.; Hagen, K. S.; Ito, M.; Kitajima, N.; Lachicotte, R. J.; Zang, Y.; Que, L., Jr. *Inorg. Chem.* **1995**, *34*, 1036−1039.

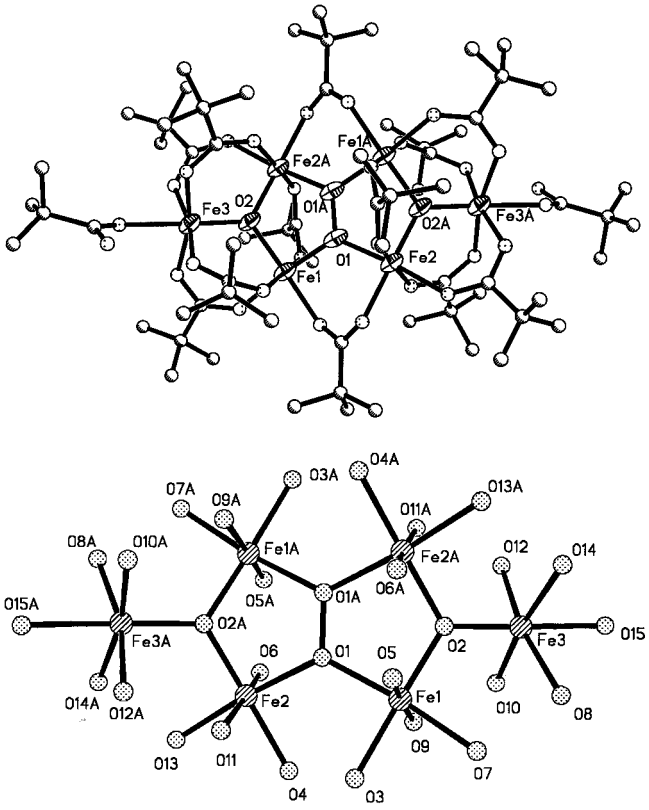

Figure 1. (top) Solid-state structure of $[Fe_6(O_2)(O)_2(O_2CCMe_3)_{12}(HO_2CCMe_3)_2]$ (**4**) showing 50% probability ellipsoids and the atom labeling scheme. (bottom) Structure of the $[Fe_6(O_2)(O)_2]$ core and first coordination sphere atoms. Selected interatomic distances (Å) and angles (deg): Fe1−O1 2.030(5), Fe1−O2 1.903(4), Fe2−O1 2.011(4), Fe2−O2A 1.907(4), Fe3−O2 1.862(4), O1−O1A 1.446(8), Fe1−O1−Fe2 127.7(2), Fe1−O1−O1A 114.7(4), Fe1−O2−Fe3 122.7(2), Fe1−O2−Fe2A 115.6(2), Fe2−O1−O1A 117.5(4), Fe2−O2A−Fe3A 121.65(19).

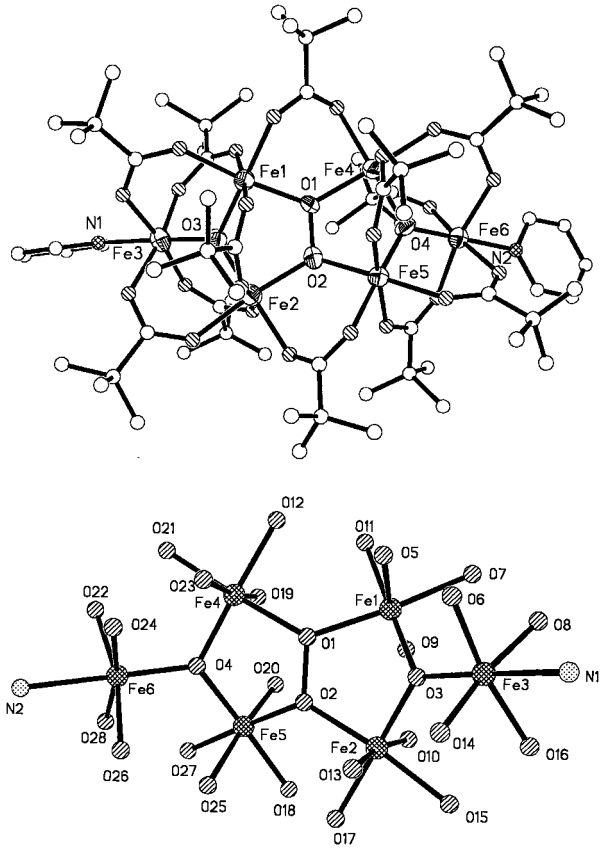

Figure 2. (top) Solid-state structure of $[Fe_6(O_2)(O)_2(O_2CCMe_3)_{12}(py)_2]\cdot 0.5Me_2CO$ (**5**) showing 50% probability ellipsoids and the atom labeling scheme. (bottom) Structure of the $[Fe_6(O_2)(O)_2]$ core and first coordination sphere atoms. Selected interatomic distances (Å) and angles (deg): Fe1−O1 2.014(7), Fe1−O3 1.914(6), Fe2−O2 2.024(7), Fe2−O3 1.898(6), Fe4−O1 2.047(6), Fe4−O4 1.901(6), Fe5−O2 2.013(7), Fe5−O4 1.918(6), Fe3−O3 1.880(6), Fe3−N1 2.196(9), Fe6−O4 1.887(6), Fe6−N2 2.231(10), O1−O2 1.522(9), Fe1−O1−Fe4 129.8(3), Fe1−O1−O2 110.9(4), Fe1−O3−Fe3 121.6(3), Fe1−O3−Fe2 116.7(3), Fe2−O2−Fe5 127.3(3), Fe2−O2−O1 117.7(5), Fe2−O3−Fe3 121.7(3), Fe4−O1−O2 116.4(5), Fe4−O4−Fe6 122.5(3), Fe4−O4−Fe5 116.0(3), Fe5−O2−O1 110.8(4), Fe5−O4−Fe6 121.5(3).

same precursor species responsible for releasing the active oxidant. The behavior of **3** is thus similar to that previously encountered[4] with the acetate congener $[Fe(O_2CCH_3)_2(py)_4]$, with the exception that, in the latter case, access to the corresponding all-ferric oxo-centered species is not attainable by virtue of dioxygen exposure.

(ii) Structures Containing the $[Fe^{III}_6(O_2)(O)_2]$ Core Unit. To further investigate the possible role of Fe^{III}_3O-containing species in the oxygenation of substrates—exemplified in oxidations of adamantane[17] and reported[27] epoxidations of olefinic acetates by $[Fe^{III}_3O(O_2CCMe_3)_6(MeOH)_3]^+$—compound $[Fe_3O(O_2CCMe_3)_6(L)_3]Cl$ (L = H_2O (**1**), py (**2**)) has been exposed to hydrogen peroxide. Starting from **1** or **2**, the hexairon(III) complex $[Fe_6(O_2)(O)_2(O_2CCMe_3)_{12}(L)_2]$ (L = Me_3CCO_2H (**4**) or py (**5**)) can be readily obtained. The solid-state structures of **4** and **5** (Figures 1 and 2) have precedent in the structure of $[Fe_6(O_2)(O)_2(O_2CPh)_{12}(H_2O)_2]$ reported by Lippard and coworkers.[30] The distinctive feature in these structures is a central η^2,μ_4-peroxo unit which, in conjunction with two pivalate moieties, bridge two $[Fe_3O(O_2CCMe_3)_5(L)]^{2+}$ units. As shown in Figure 3, the $[Fe_6(O_2)(O)_2]$ core units of **4** and **5** are structurally different, the former adopting a recliner conformation with an almost planar $[Fe_4(O_2)]$ central unit and the latter exhibiting a "butterfly"-like conformation with substantial twist of the "body" $[Fe_4(O_2)]$ component. By virtue of a crystallographically imposed inversion center in the structure of **4**, the symmetry-related pivalates bridging between Fe1 and Fe2A, and Fe2 and Fe1A, lie on opposite sites of the $[Fe_4(O_2)]$ core. In contrast, the corresponding pivalates in the structure of **5**, which lacks any rigorous symmetry element, reside on the same side of the core surface. The resulting steric encumbrance, which is primarily due to the bulky *tert*-butyl substituents, is apparently relaxed via the twist of the $[Fe_4(O_2)]$ core in **5**. The observed O−O bond distances (O1−O1A 1.446(8) (**4**); O1−O2 1.522(9) Å (**5**)) are characteristic of peroxo bond lengths, and are comparable to the O−O distance (1.480(12) Å) reported[30] for the benzoate analogue. Within the $[Fe_4(O_2)]$ core unit, the average Fe−O bond distances (2.02 (1) (**4**), 2.03(2) (**5**), 2.01(1) Å (benzoate analogue)) are closely spaced in a typical range for ferric sites. The longer O−O bond distance in **5** is most likely associated to the distortion (twist) of the Fe_4 core disposition noted above.

To explore whether any systematic changes in electronic parameters may influence the O−O bond distance, an electron-withdrawing carboxylate was chosen to replace as many pivalates as possible in the hexairon(III) peroxo structure. The reaction of **4** with CF_3COOH (12−20 equiv over **4**) yields red-black crystals of $[Fe_6(O_2)(O)_2(O_2CCMe_3)_2(O_2CCF_3)_{10}(H_2O)_2]\cdot 2Me_2CO\cdot EtOH$ (**6**). The solid-state structure of **6** (Figure 4)

(30) Micklitz, W.; Bott, S. G.; Bentsen, J. G.; Lippard, S. J. *J. Am. Chem. Soc.* **1989**, *111*, 372−374.

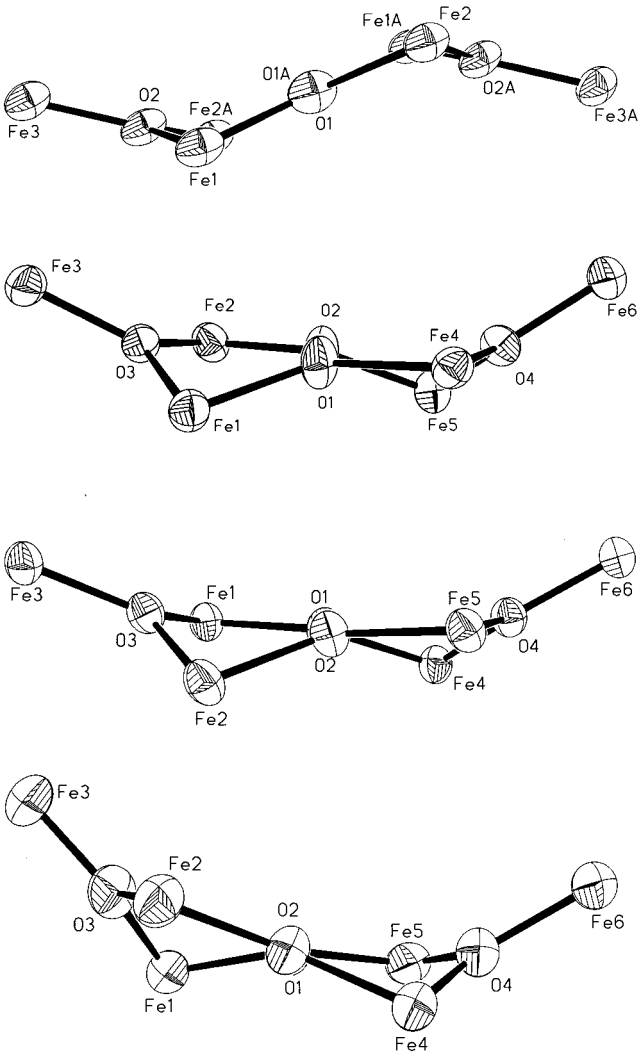

Figure 3. Conformation of the $[Fe(O_2)(O)_2]$ core in compounds, from top to bottom, **4**, **5**, **6**, and **10**.

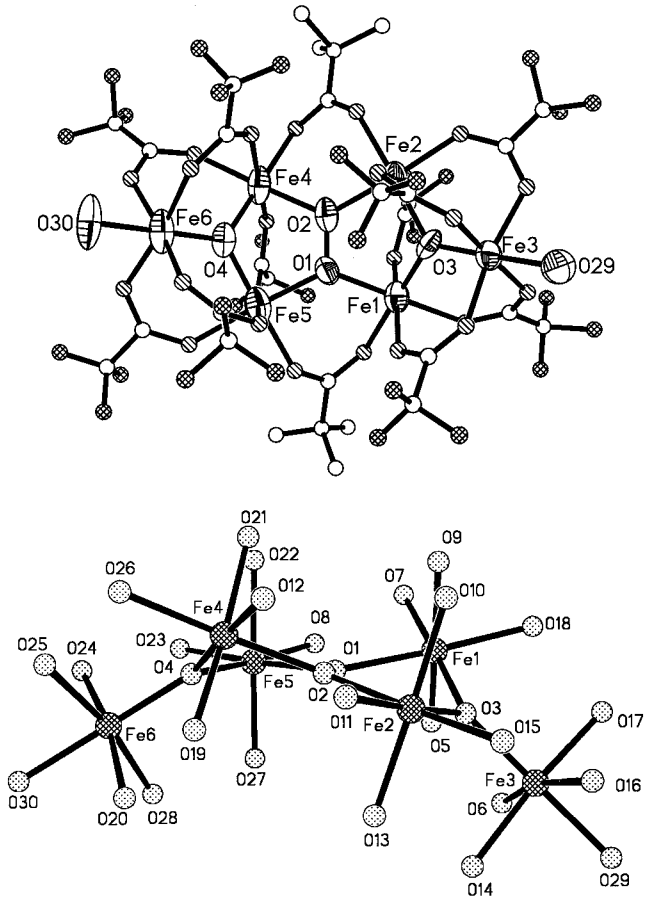

Figure 4. (top) Structure of $[Fe_6(O_2)(O)_2(O_2CCMe_3)_2(O_2CCF_3)_{10}(H_2O)_2]\cdot 2Me_2CO\cdot EtOH$ (**6**) showing 50% probability ellipsoids and the atom labeling scheme (cross-line shaded atoms are F). (bottom) Structure of the $[Fe_6(O_2)(O)_2]$ core and first coordination sphere atoms. Selected interatomic distances (Å) and angles (deg): Fe1−O1 2.020(10), Fe1−O3 1.907(10), Fe2−O2 2.026(10), Fe2−O3 1.927(9), Fe4−O2 2.013(10), Fe4−O4 1.906(11), Fe5−O1 2.012(10), Fe5−O4 1.924(11), Fe3−O3 1.878(10), Fe3−O29 2.045(10), Fe6−O4 1.876(10), Fe6−O30 2.058(10), O1−O2 1.447(13), Fe1−O1−Fe5 130.6(5), Fe1−O1−O2 110.2(7), Fe1−O3−Fe3 123.4(5), Fe1−O3−Fe2 114.5(5), Fe2−O2−Fe4 129.0(6), Fe2−O2−O1 117.2(7), Fe2−O3−Fe3 121.8(5), Fe4−O2−O1 113.7(7), Fe4−O4−Fe6 124.2(6), Fe4−O4−Fe5 114.4(5), Fe5−O1−O2 116.9(7), Fe5−O4−Fe6 121.1(6).

reveals that all pivalate moieties in **4** have been replaced by trifluoroacetate groups, with the notable exception of the two pivalates which bridge the two $[Fe_3O(O_2CCF_3)_5(H_2O)]^{2+}$ units. Use of a large excess of CF_3COOH has not yielded isolable products; hence it is currently unknown whether the retention of the two pivalate groups is a persistent feature. Despite the drastic change in the nature of the supporting carboxylate, the O−O bond length (1.447(13) Å) and average Fe−O bond distance (2.02(1) Å) within the $[Fe_4(O_2)]$ core of **6** remain virtually identical with those revealed in the structure of **4**. However, the conformation of the central $[Fe_4(O_2)]$ core (Figure 3) is more structurally akin to that observed in **5**, leaving open the possibility that any elongation of the O−O bond, due to distortion of the core unit, may have been counterbalanced via withdrawal of antibonding electron density from the peroxo unit. ^{1}H NMR data suggest that all hexairon species noted above retain their structure in solution (CD_2Cl_2 or $CDCl_3$), since resonances for all distinct and/or symmetry-related pivalates are resolved in the ^{1}H NMR spectra of compounds **4**−**6**.

(iii) Reductions/Oxidations of the Peroxo-Containing Complexes. Attempts to generate structural variants bearing more than one peroxo unit, by following methodology successfully implemented[31] in the synthesis of the unique hexairon(III) compound $[Fe_6(O_2)_3(O)_2(OAc)_9]^-$, has led to reduction of the peroxo moiety. Indeed, the reaction of **4** with a combination of H_2O_2 and NaOMe affords $[Na_2Fe_4(O)_2(O_2CCMe_3)_{10}(CH_3CN)(Me_2CO)]$ (**7**). Essentially the same species is also derived upon treatment of the peroxo complex **4** with $NaBH_4$ in CH_2Cl_2, leading to isolation of $[Na_2Fe_4(O)_2(O_2CCMe_3)_{10}(HO_2CCMe_3)_2]\cdot 4CH_2Cl_2$ (**8**). The solid-state structures of **7** and **8** (Figures 5 and 6) reveal a central $[Na_2Fe_4(O)_2]$ core, featuring a variation of the well-documented[32] bent ("butterfly") arrangement of four ferric sites in $[Fe_4(\mu_3\text{-}O)_2]$ units. Indeed, the μ_4-O bridges in the present structures are not only associated with three basal ferric sites but also with a sodium atom (average Na−O 2.463 (**7**), 2.460 (**8**) Å) in an overall tetrahedral coordination, distorted toward a trigonal pyramidal geometry (Na atom on the apex). The angles between the plane of the central ("body") Fe_2O_2

(31) Shweky, I.; Pence, L. A.; Papaefthymiou, G. C.; Sessoli, R.; Wun, J. W.; Bino, A.; Lippard, S. J. *J. Am. Chem. Soc.* **1997**, *119*, 1037−1042.

(32) (a) Wemple, M. W.; Coggin, D. K.; Vincent, J. B.; McCusker, J. K.; Streib, W. E.; Huffman, J. C.; Hendrickson, D. N.; Christou, G. *J. Chem. Soc., Dalton Trans.* **1998**, 719−725. (b) McKusker, J. K.; Vincent, J. B.; Schmitt, E. A.; Mino, M. L.; Shin, K.; Coggin, D. K.; Hagen, P. M.; Huffman, J. C.; Christou, G.; Hendrickson, D. N. *J. Am. Chem. Soc.* **1991**, *113*, 3012−3021. (c) Gorun, S. M.; Lippard, S. J. *Inorg. Chem.* **1988**, *27*, 149−156. (d) Armstrong, W. H.; Roth, M. E.; Lippard, S. J. *J. Am. Chem. Soc.* **1987**, *109*, 6318−6326.

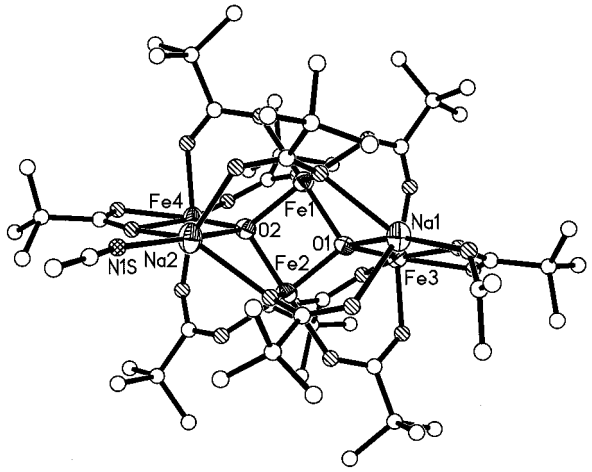

Figure 5. Solid-state structure of $[Na_2Fe_4(O)_2(O_2CCMe_3)_{10}(CH_3CN)(Me_2CO)]$ (**7**) showing 50% probability ellipsoids and the atom labeling scheme. Selected interatomic distances (Å) and angles (deg): Fe1−O1 1.979(5), Fe1−O2 1.943(4), Fe2−O1 1.947(4), Fe2−O2 1.974(5), Fe3−O1 1.841(5), Fe4−O2 1.859(4), Na1−O1 2.482(5), Na2−O2 2.443(5), Fe1···Fe2 2.9331(15), O1−Fe1−O2 82.93(18), O1−Fe2−O2 82.97(18), Fe1−O3−Fe3 123.4(5), Fe1−O2−Fe2 96.96(18), Fe1−O1−Fe2 96.70(19), Fe1−O2−Fe4 121.1(2), Fe1−O2−Na2 116.4(2), Fe4−O2−Na2 97.40(18), Fe1−O1−Fe3 125.2(2), Fe1−O1−Na1 100.04(19), Fe3−O1−Na1 98.33(19).

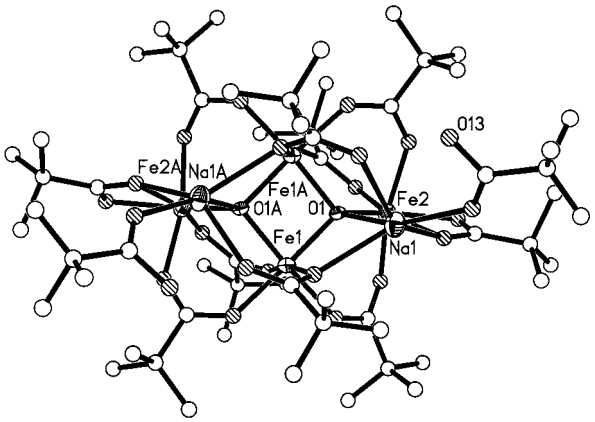

Figure 6. Solid-state structure of $[Na_2Fe_4(O)_2(O_2CCMe_3)_{10}(HO_2CCMe_3)_2]\cdot 4CH_2Cl_2$ (**8**) showing 50% probability ellipsoids and the atom labeling scheme. Selected interatomic distances (Å) and angles (deg): Fe1−O1 1.971(4), Fe1−O1A 1.960(4), Fe2−O1 1.850(4), Na1−O1 2.460(5), Fe1···Fe1A 2.941(2), O1−Fe1−O1A 83.06(18), Fe1−O1−Fe1A 96.89(18), Fe1−O1−Fe2 125.6(2), Fe1−O1−Na1 104.1(2), Fe2−O1−Na1 95.92(19).

rhomb (maximum deviation from a least-squares fit plane is 0.0428 Å) and the attendant ("wing") planes defined by atoms Na2−O2−Fe4 and Na1−O1−Fe3 (**7**) are nearly orthogonal. Metrical parameters for the bent $[Fe_4(O)_2]$ unit are within the range of characteristic bond length and angle values tabulated by Gorun and Lippard.[32c] The $[Na_2Fe_4(O)_2]$ core is further fortified by virtue of eight bridging pivalate groups, two of which are fairly unique, as they span the range between the two sodium ions, while also coordinating via one oxygen atom (shared by a Na and an Fe) to one of the "body" iron sites. The other six pivalate groups provide one or two bridges between "wing-tip" and "body" iron centers, the number of bridges alternating around the $[Fe_4(O)_2]$ unit. Two more pivalate groups bridge the corresponding "wing-tip" iron and sodium atoms. Finally, a neutral donor molecule, either acetone/acetonitrile (**7**) or pivalic acid (**8**), completes the coordination sphere of each Na atom. Due to the presence of the same neutral molecule in

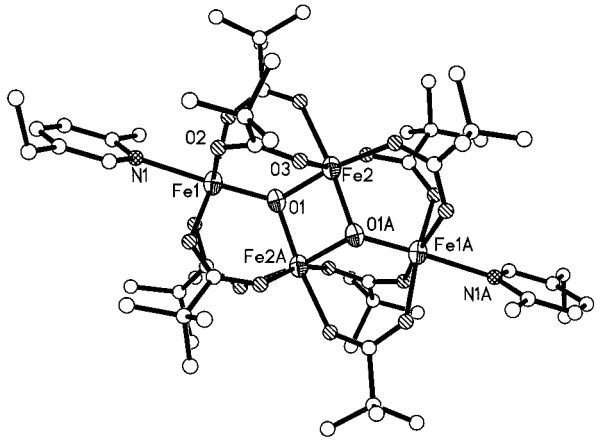

Figure 7. Solid-state structure of $[Fe_4(O)_2(O_2CCMe_3)_8(2\text{-Me-5-Etpy})_2]\cdot 2CH_3CN$ (**9**) showing 50% probability ellipsoids and the atom labeling scheme. Selected interatomic distances (Å) and angles (deg): Fe1−O1 1.836(5), Fe1−N1 2.227(6), Fe1−O2 2.039(5), Fe2−O1 1.931(5), Fe2−O1A 1.936(5), Fe2−O3 2.056(5), Fe2···Fe2A 2.942(2), O1−Fe1−O2 99.2(2), O1−Fe1−N1 172.3(2), Fe1−O1−Fe2 123.2(3), Fe1−O1−Fe2A 123.1(3), Fe2−O1−Fe2A 99.1(2), O1−Fe2−O1A 80.9(2), O1−Fe2−O3 94.4(2).

8, the overall symmetry of the structure is higher, retaining a 2-fold rotational axis penetrating the center of the $[Fe_2(O)_2]$ rhomb.

Chemical and electrochemical oxidations of the peroxo-containing species were also attempted in efforts directed toward stabilizing high-valent iron oxo or peroxo units. Cyclic voltammograms of $[Fe_6(O_2)(O)_2(O_2CCMe_3)_{12}(HO_2CCMe_3)_2]$ (**4**) were generally indicative of facile destruction of the $[Fe_6(O_2)(O)_2]$ core. This was further confirmed in chemical oxidations of **4** with $[NH_4]_2[Ce(NO_3)_6]$ in $EtOH/H_2O$, which afford quantitatively $[Fe_3O(O_2CCMe_3)_6(EtOH)_2(H_2O)](NO_3)\cdot CH_3CH_2OH$ (the structure of this compound is available as Supporting Information). A similar $Fe^{III}{}_3O$-containing cation, $[Fe_3O(O_2CCMe_3)_6(thf)_3]^+$, is obtained upon treatment of **4** with $NOBF_4$ in diethyl ether, followed by recrystallization of the product from thf/hexane. Apparently, the peroxide bridge is the only site affected in these redox reactions, although its exact fate has not been determined.

(iv) Employment of 2-Methyl-5-ethylpyridine. To investigate the effect of bulky ligands which can potentially provide five-coordinate ferrous sites to facilitate dioxygen activation, the electron-rich, but sterically demanding, 2-methyl-5-ethylpyridine was employed in conjunction with pivalic acid. A mixture of iron powder and pivalic acid (2 equiv over Fe) in 2-Me-5-Etpy affords, after prolonged stirring, a yellow-green solution, from which an exceedingly air-sensitive material was obtained. Unfortunately, we were unable to handle this ferrous species using standard Schlenk techniques, especially in solvents other than 2-Me-5-Etpy.

Access to a starting all-ferric species bearing 2-Me-5-Etpy as a ligand can be provided by dissolving $[Fe_3O(O_2CCMe_3)_6(H_2O)_3]Cl$ (**1**) in 2-Me-5-Etpy. Surprisingly, **1** does not transform to the corresponding pyridine adduct, but rather rearranges to yield $[Fe_4(O)_2(O_2CCMe_3)_8(2\text{-Me-5-Etpy})_2]\cdot 2CH_3CN$ (**9**) as red-black crystals from acetonitrile. The structure of **9** (Figure 7) reveals a central $[Fe_4(O)_2]$ core which possesses planar disposition of the four metal sites, leaving the two symmetry related μ_3-O bridging atoms at opposite sides of the Fe_4 plane, at a distance of 0.412 Å. This arrangement of the $[Fe_4(O)_2]$ core is documented[32] in the structure of the archetypal $[Fe_4(O)_2(O_2CCF_3)_8(H_2O)_6]$. Two pivalate groups bridge each ferric site of

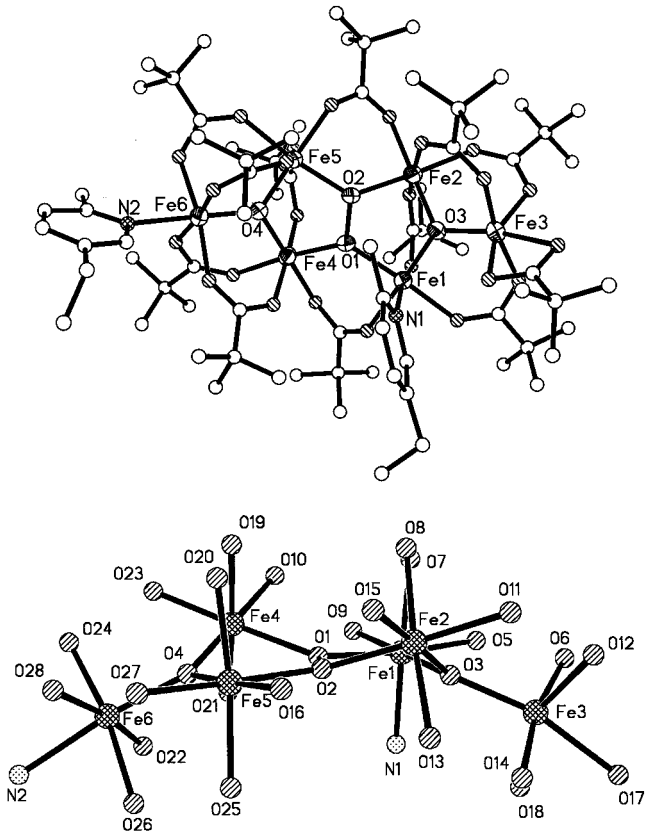

Figure 8. (top) Solid-state structure of $[Fe_6(O_2)(O)_2(O_2CCMe_3)_{12}(2\text{-Me-5-Etpy})_2]$ (**10**) showing 50% probability ellipsoids and the atom labeling scheme. (bottom) Structure of the $[Fe_6(O_2)(O)_2]$ core and first coordination sphere atoms. Selected interatomic distances (Å) and angles (deg): Fe1−O1 2.045(3), Fe1−O3 1.884(3), Fe2−O2 2.016(3), Fe2−O3 1.940(3), Fe4−O1 2.036(3), Fe4−O4 1.905(3), Fe5−O2 2.038(3), Fe5−O4 1.895(3), Fe3−O3 1.892(3), Fe1−N1 2.206(4), Fe6−O4 1.894(3), Fe6−N2 2.255(4), O1−O2 1.475(4), Fe1−O1−Fe4 129.59(14), Fe1−O1−O2 116.25(18), Fe1−O3−Fe3 126.31(15), Fe1−O3−Fe2 114.32(14), Fe2−O2−Fe5 128.76(13), Fe2−O2−O1 111.95(19), Fe2−O3−Fe3 118.52(14), Fe4−O1−O2 111.71(18), Fe4−O4−Fe6 122.58(14), Fe4−O4−Fe5 115.69(14), Fe5−O2−O1 116.61(18), Fe5−O4−Fe6 121.72(14), O1−Fe1−N1 97.39(13), O3−Fe1−N1 97.37(12), O4−Fe6−N2 174.45(13).

the inner $[Fe_2(O)_2]$ core to each distal iron site, yielding a total of eight symmetry-related (by inversion) pivalate moieties supporting the $[Fe_4(O)_2]$ unit. A unique 2-Me-5-Etpy moiety completes the coordination sphere of each distal ferric site at position trans to the bridging oxo moiety.

Exposure of **9** to hydrogen peroxide affords $[Fe_6(O_2)(O)_2(O_2CCMe_3)_{12}(2\text{-Me-5-Etpy})_2]$ (**10**) as reddish-black crystals from diethyl ether. The compound exhibits an asymmetric structure (Figure 8) which, otherwise, is similar to those documented above for peroxo species that feature distorted $[Fe_6(O_2)(O)_2]$ cores (Figure 3). The source of the asymmetry is the migration of a single 2-Me-5-Etpy moiety from its anticipated coordination at a distal ferric site (Fe3), to a ferric center (Fe1) belonging to the central $[Fe_4(O_2)]$ unit. This is accompanied by a shift of a pivalate group from a potentially bridging position between Fe3 and Fe1 to a chelating coordination mode of the distal Fe3 site. The origins of these molecular translocations (not observed at the other end of the molecule) are not clearly understood, but presumably involve alleviation of steric hindrance between the two halves of the molecule.

Oxygenation of Substrates. Stoichiometric Reactions of Peroxo-Containing Species. The possibility that the peroxo moiety observed in a number of complexes containing the $[Fe_6(O_2)(O)_2]$ unit may be involved in oxo transfer and/or hydrogen-abstraction chemistry was explored with *cis*-stilbene and adamantane, respectively.

cis-Stilbene undergoes oxygenation by either **4** or **5**, albeit at very slow rates. The reaction of **4** or **5** with *cis*-stilbene (3.3 μmol, 1 equiv over **4**/**5**) in C_6D_6 (70 °C) under N_2 was followed by ^{1}H NMR to reveal the generation of benzaldehyde and *trans*-stilbene oxide over a period of several weeks. Conversions in the presence of **5** (which exhibits a weaker O−O bond than **4**) are somewhat better, but even after 8 weeks, only 0.3 μmol of benzaldehyde and 0.5 μmol of *trans*-stilbene oxide are obtained (20% yield). These amounts double if **5** is allowed to react with 2 equivalents of *cis*-stilbene (7 μmol). The products are most likely formed due to direct interaction of *cis*-stilbene with the peroxo unit of **4** or **5**. An attempt to use $[Fe_3O(O_2CCMe_3)_6(py)_3]Cl$ (**2**) (20 mg, 0.022 mmol) to oxygenate *cis*-stilbene (0.2 mL), employed as both substrate and solvent, afforded no products in the presence of O_2 under 50 °C for 20 h. Apparently, the reported[27] use of $[Fe_3O(O_2CCMe_3)_6(MeOH)_3]Cl$ to mediate epoxidation of olefinic acetates under similar conditions may depend on the ability of these functionalized olefins to generate substrate-centered hydroperoxides, which in turn are activated by the catalyst to support epoxidation.

Stoichiometric oxidations of adamantane (14 mg, 0.10 mmol) by **5** (0.10 mmol) in py/PivH (10 g/1 g) afford no detectable oxygenation products under ambient conditions during periods (18 h) typically used in Gif catalysis. However, upon heating at 66 °C for 3 days, very low yields of 1-ol (0.4 μmol), 2-one (0.4 μmol), 2-(1-Ad)py (0.9 μmol), and 2-(2-Ad)py (0.1 μmol) are obtained. The presence of adamantylpyridines denotes the intermediacy of adamantyl radicals, and hence the ability of the active oxidant to perform hydrogen-atom abstraction. However, the *tert*/*sec* selectivity obtained (≈8) suggests that a more selective oxidant (probably the peroxo unit per se, or a hydroperoxo version) is involved in these low-yield oxidations by comparison to product profiles (tert/sec = 3−5) obtained[17] from catalytic oxygenations of adamantane (Fe_{cat} (**2**, **3**, or $[Fe_3O(O_2CCMe_3)_6(py)_3]/Zn/O_2$). Therefore, the reactivity and selectivity of the stoichiometric oxygenations suggest that the present class of peroxo units does not contribute directly to the outcome of those catalytic versions. Apparently, the catalytic reactions are mediated by a combination of HO$^\bullet$ and RO$^\bullet$ radicals (R = adamantyl), in which RO$^\bullet$ radicals are prominently represented due to the obligatory presence of O_2 ($R^\bullet + O_2 \rightarrow ROO^\bullet \rightarrow RO^\bullet$). We are currently investigating whether Zn may also play a role by reductively quenching HO$^\bullet$ more efficiently than RO$^\bullet$ radicals.

Summary

The following are the principal findings of the present study:

(1) Compounds of the pivalic acid anion with Fe(II), mixed-valent Fe(II/III), and Fe(III) sites can be readily prepared starting from the triiron μ_3-oxo bridged species $[Fe_3O(O_2CCMe_3)_6(L)_3]^{+/0}$ (L = H_2O, py). These complexes include the air-sensitive $[Fe^{II}(O_2CCMe_3)_2(py)_4]$ (**3**), which can be produced by reduction of the known mixed-valent compound $[Fe_3O(O_2CCMe_3)_6(py)_3]$ with Zn in pyridine/pivalic acid, or directly by dissolving Fe metal in the presence of 2 equiv of pivalic acid in pyridine. Compound **3** is readily oxidized to $[Fe_3O(O_2CCMe_3)_6(py)_3]$ by dioxygen, which is slowly converted to the all-ferric $[Fe_3O(O_2CCMe_3)_6(py)_3]^+$. All three reagents support oxygenation of adamantane by Zn/O_2 in pyridine/pivalic acid (10:1 w/w).

(2) Treatment of $[Fe_3O(O_2CCMe_3)_6(L)_3]^+$ (L = H_2O (**1**), py (**2**)) with H_2O_2 generates the peroxo-containing hexairon(III) species $[Fe_6(O_2)(O)_2(O_2CCMe_3)_{12}(L)_2]$ (L = Me_3CCO_2H (**4**),

py (**5**)), which feature the previously documented $[Fe_6(\eta^2,\mu_4\text{-}O_2)(\mu_3\text{-}O)_2]$ core. The same core unit is also observed in $[Fe_6(O_2)(O)_2(O_2CCF_3)_{10}(O_2CCMe_3)_2(H_2O)_2]$ (**6**), obtained by replacing all pivalates in **4** by trifluoroacetates, with the exception of those pivalates bridging between the two $[Fe_3O(O_2CCF_3)_5(H_2O)]$ units.

(3) Reduction of **4** with $NaBH_4$ (or NaOMe) results in the formation of $[Na_2Fe_4(O)_2(O_2CCMe_3)_{10}(L)(L')]$ ($L = CH_3CN$, $L' = Me_2CO$ (**7**); $L = L' = Me_3CCO_2H$ (**8**)), which reveals a variation of the bent ("butterfly") $[Fe_4(O)_2]$ core. In contrast, oxidation of **4** with Ce^{IV} or $[NO]^+$ regenerates the triangular μ_3-oxo bridged $[Fe_3O(O_2CCMe_3)_6(solv)_3]^+$ (solv = EtOH, H_2O, thf). A similar $[Fe_4(O)_2]$ core, albeit planar, is observed in $[Fe_4(O)_2(O_2CCMe_3)_8(2\text{-Me-5-Etpy})_2]$ (**9**) generated in attempts to replace H_2O by the sterically demanding pyridine, 2-Me-5-Etpy, in $[Fe_3O(O_2CCMe_3)_6(H_2O)_3]^+$. Compound **9** is transformed by H_2O_2 to the hexairon(III) peroxo species $[Fe_6(O_2)(O)_2(O_2CCMe_3)_{10}(2\text{-Me-5-Etpy})_2]$ (**10**), which contains an $[Fe_6(O_2)(O)_2]$ core unit similar to those noted above, although the overall structure is asymmetric due to translocation of one pyridine from a distal Fe site to an Fe belonging to the $[Fe_4(O_2)]$ inner core.

(4) Stoichiometric reactions of **4** and **5** with hydrocarbons in benzene or py/PivH indicate that very low yields of oxo products are obtained with *cis*-stilbene (benzaldehyde, *trans*-stilbene oxide) and adamantane (1-ol, 2-one, 2-(1-Ad)py, 2-(2-Ad)py) upon prolonged heating. In the latter case, the tert/sec selectivity obtained differs from that observed in catalytic Gif-type oxygenations of adamantane supported by O_2/Zn (or H_2O_2). We thus conclude that the present peroxo species do not directly participate as active oxidants in those catalytic reactions.

Acknowledgment. The present work was generously supported by grants from the NIH/NIEHS (2 P42 ES07381-06), the U.S. Environmental Protection Agency (R823377-01-1), and the donors of the Petroleum Research Fund administered by the American Chemical Society (ACS-PRF-29383-G3).

Supporting Information Available: Tables S1−S50 containing listings of crystal data and structure refinement, atomic coordinates and equivalent isotropic displacement parameters, interatomic distances and bond angles, anisotropic displacement parameters, and hydrogen coordinates and isotropic displacement parameters for compounds **1**, **3**−**10**, and $[Fe_3O(O_2CCMe_3)_6(EtOH)_2(H_2O)](NO_3)\cdot EtOH$ (along with an ORTEP diagram). This material is available free of charge via the Internet at http://pubs.acs.org.

IC000261+